JPL PUBLICATION 85-25

Optical Receivers Using Rough Reflectors

Victor A. Vilnrotter

May 1, 1985

National Aeronautics and
Space Administration

Jet Propulsion Laboratory
California Institute of Technology
Pasadena, California

The research described in this publication was carried out by the Jet Propulsion Laboratory, California Institute of Technology, under a contract with the National Aeronautics and Space Administration.

ABSTRACT

This report examines the possible use of "rough," or nondiffraction-limited, reflectors for collecting optical signals. It is shown that in the absence of background radiation, the reflector's surface quality has little effect on the performance of a properly designed receiver, but that the presence of even small amounts of background radiation can lead to severe performance degradation. Techniques are suggested for improving receiver performance in high-background environments, and bounds and approximations to the exact error-probability expressions are derived.

ACKNOWLEDGMENTS

The author wishes to thank Eugene R. Rodemich for helping with the proof in Appendix B, and James R. Lesh for suggesting improvements to the original manuscript.

CONTENTS

1. INTRODUCTION 1-1

2. OPTICAL RECEIVER CHARACTERISTICS 2-1

3. OPTICAL RECEIVER PERFORMANCE 3-1

3.1 DECODER STRUCTURE 3-1

3.2 DECODER PERFORMANCE 3-4

3.3 BOUNDS AND APPROXIMATIONS 3-6

4. NUMERICAL RESULTS 4-1

4.1 RECEIVER PERFORMANCE 4-1

4.1.1 No Background Radiation 4-1

4.1.2 The Effects of Background Radiation 4-3

4.1.3 Focal-Plane Detector Arrays 4-7

4.2 PERFORMANCE BOUNDS AND APPROXIMATIONS 4-11

5. CONCLUDING REMARKS 5-1

6. REFERENCES 6-1

APPENDIXES

A. A-1

B. B-1

Figures

2-1. Optical Receiver Components 2-2

2-2. Fractional Signal Power $F(\theta)$ as a Function of θ for Various System Parameters:

(a) $\sigma = 0.03$ μm, $T_c = 0.25$ m, and $\lambda = 1$ μm 2-5

(b) $R = 5$ m, $T_c = 0.5$ m, and $\lambda = 1$ μm 2-6

(c) $\sigma = 0.07$ μm, $R = 5$ m, and $\lambda = 1$ μm 2-7

4-1. Symbol Error Probability ${}_NP_M(E)$ as a Function of θ, with No Background Radiation 4-2

4-2. Symbol Error Probability ${}_NP_M(E)$ as a Function of θ in the Presence of Background Radiation 4-4

4-3. Minimum Symbol Error Probability as a Function of K_{so} for:

(a) Various Background Levels 4-5

(b) Various rms Surface Deviations 4-6

4-4. Minimum Error Probability as a Function of K_{so} for Optimized Single-Detector (N = 1) and Partitioned Field-of-View (N = 2) with:

(a) Moderate Background Level, M = 2 4-8

(b) High Background Level, M = 32 4-9

(c) Fractional Signal Power vs. θ for Cases Considered in Figures 4-4(a) and (b) 4-10

4-5. Performance Bounds and Approximations with:

(a) M = 2 4-12

(b) M = 32 4-13

4-6. Symbol Error Probability Approximations for a Partitioned Field-of-View with:

(a) M = 2 4-14

(b) M = 32 4-15

SECTION 1

INTRODUCTION

The development and eventual deployment of large, Earth-orbiting optical receivers is under consideration at the present time. Such receivers could be used to detect weak optical signals from distant deep-space vehicles, or to relay high-rate optical data from nearby planetary probes (and other near-Earth sources) to the ground. From a communications viewpoint, one of the most important parameters of an optical receiver is its effective aperture, which determines the amount of signal power the receiver can extract from an incident signal field. Diffraction-limited optical reflectors provide the greatest protection against background interference, allowing the minimization of the receiver's field-of-view. However, it is generally both difficult and costly to construct large, diffraction-limited reflectors at optical wavelengths, hence our interest in the potential use of "rough" reflectors for optical communications. Thus, multielement reflectors designed for coherent operation at infrared wavelengths could be employed in a "photon-bucket" mode at much higher frequencies, or large, inexpensive reflectors with poor optical surface quality may at times be employed to collect signal energy. Since "rough" reflectors typically scatter a significant fraction of the incident signal field, special processing techniques must be used to recover the scattered signal energy to improve receiver performance.

The following sections address some of the fundamental issues associated with the use of nondiffraction-limited reflectors for optical communications. In Section 2, a useful model for signal and background intensity distributions is developed. The structure and performance of a minimum error-probability, direct-detection optical receiver is derived in

Section 3, along with bounds and approximations to the exact expressions. Finally, in Section 4, numerical examples are provided to illustrate receiver performance under various operating conditions of interest, and to provide insight into the use of bounds and approximations developed in the previous section.

SECTION 2

OPTICAL RECEIVER CHARACTERISTICS

The class of optical receivers considered in this report consists of the following basic optical components: a reflector (of radius R and focal length f) designed to collect and focus optical fields, a narrowband optical filter (passband $[\lambda, \lambda + \Delta\lambda)$) designed to pass the signal fields but reject out-of-band background radiation, a spatial filter to limit the receiver's field-of-view, an optical detector array to convert the impinging optical fields into electrical signals, and a post-detection processor to attempt to reconstruct the transmitted message with the desired fidelity. The arrangement of these components is shown in Figure 2-1.

The reflector's surface can be modeled as an isotropic random function with normal height distribution above and below the mean surface. Let the random variable h denote the deviation of the actual surface from its mean value at a particular point on the reflector, and let τ_c be the distance between two points on the surface. It is generally assumed [Refs. 1 and 2] that h is Gaussian with probability density

$$p(h) = \frac{1}{\sqrt{2\pi}\ \sigma} e^{-h^2/2\sigma^2} \tag{2.1}$$

and that the correlation function along the surface is of the form

$$C(\tau_c) = e^{-\tau_c^2/T_c^2} \tag{2.2}$$

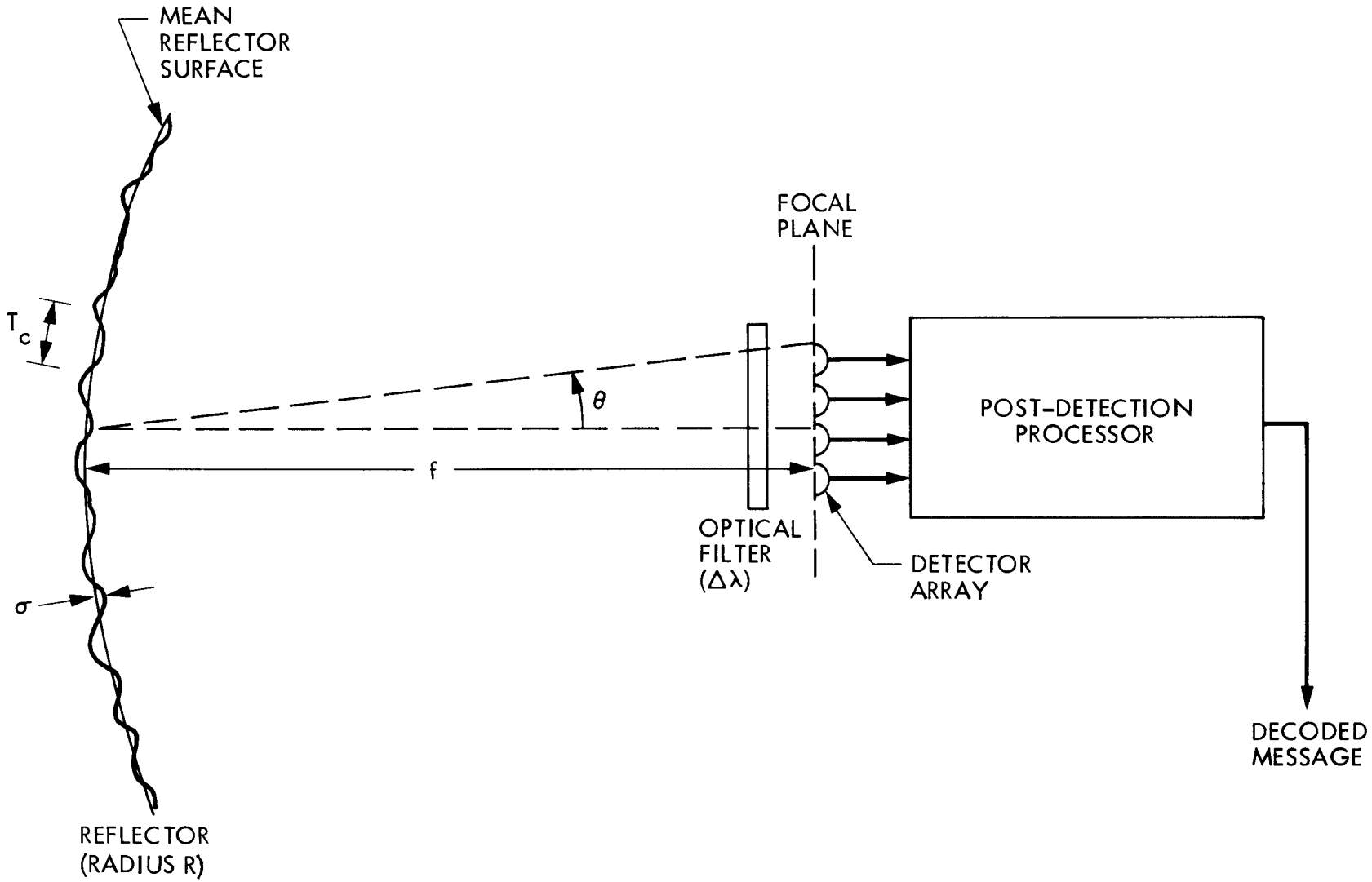

Figure 2-1. Optical Receiver Components

Thus, σ is the root-mean-square (rms) surface deviation, and T_c is the correlation length averaged over all directions along the surface.

A point in the focal plane can be specified by its Cartesian coordinates (x,y), or, equivalently, by its polar coordinates (θ,ϕ) (for small θ, $\theta \simeq \sqrt{x^2 + y^2}/f$ and ϕ is the angle between the vector $\underline{r} = x\hat{i} + y\hat{j}$ and one of the Cartesian axes). If a circular reflector with rms surface deviation σ and correlation length T_c is illuminated by a normally incident plane-wave, then the fraction of power passing through a circular aperture of radius θf centered in the focal-plane is given by the expression [Ref. 2]

$$F(\theta) = F_1(\theta) + F_2(\theta) \tag{2.3a}$$

where

$$F_1(\theta) = e^{-g}\left\{1 - \left(J_o^2(kR\theta) + J_1^2(kR\theta)\right)\right\}, \tag{2.3b}$$

$$F_2(\theta) = 1 - e^{-g}\left\{1 + \sum_{m=0}^{\infty} \frac{g^m}{m!}\, e^{-(kT_c\theta/2)^2/m}\right\}, \tag{2.3c}$$

$$g = \left(\frac{4\pi\ \sigma}{\lambda}\right)^2 \tag{2.3d}$$

(λ is the center wavelength of the optical signal, and $k \triangleq 2\pi/\lambda$.) It is apparent that $F_1(\theta)$ is the contribution of the Airy pattern generated by the mean reflector surface, attenuated by an exponential function that depends on σ, while $F_2(\theta)$ describes the distribution of power scattered out of the Airy pattern (note that $F_2(\theta)$ is independent of the reflector radius). For a "rough reflector" $g >> 1$, and $F(\theta)$ can be approximated as [Ref. 2]

$$F(\theta) \simeq 1 - e^{-\frac{1}{8}(\theta/\theta_0)^2} \qquad ; g >> 1 \tag{2.4}$$

where

$$\theta_0 \triangleq \sqrt{2}\ \sigma/T_c$$

The behavior of $F(\theta)$ is examined in Figure 2-2 for various combinations of R, σ, and T_c at a wavelength of $\lambda = 1$ μm. For $g \ll 1$, the enclosed power depends strongly on the reflector radius R, as shown in Figure 2-2(a). As σ (and hence g) increases, the contribution of the Airy pattern becomes less important (see Figure 2-2(b)). For large values of g (corresponding to $\sigma = 0.2$ μm), the contribution of the Airy pattern becomes negligible and the approximation of Equation 2.4 may be used. Note that for a given rms surface deviation, the amount of power scattered out of the Airy pattern does not vary significantly as the correlation length changes, but the actual distribution of scattered energy does (see Figure 2-2(c)).

Equation 2.3a can be used to relate the power reaching the detector array to the intensity of the optical field at the receiver. If the intensity of a normally incident plane-wave at the receiver is I_r W/m^2, then the power passing through a circular aperture of radius θf in the focal plane is

$$P_s(\theta) = A_r I_r\ F(\theta) \tag{2.5}$$

in watts, where $A_r \triangleq t_s\ \pi\ R^2$ is the effective aperture of the reflector (t_s is the bulk power transmission factor of the receiver, with $0 < t_s \leq 1$). Background radiation may also enter the receiver along with the desired signal field. This type of radiation is generally of thermal origin, and it may be due entirely to self-emission by hot sources (such as stars) or it may be a combination of self-emission and reflected radiation (as from planets). With the exception of the Sun, stars generally appear as point sources due to their great distance from the receiver, while planets appear as distributed sources to receivers capable of resolving their disks. Here we consider only extended background sources that are characterized by a spatially constant spectral radiance function, $N(\lambda)$ (the units of $N(\lambda)$ are W/m^2-μm-sr). The power

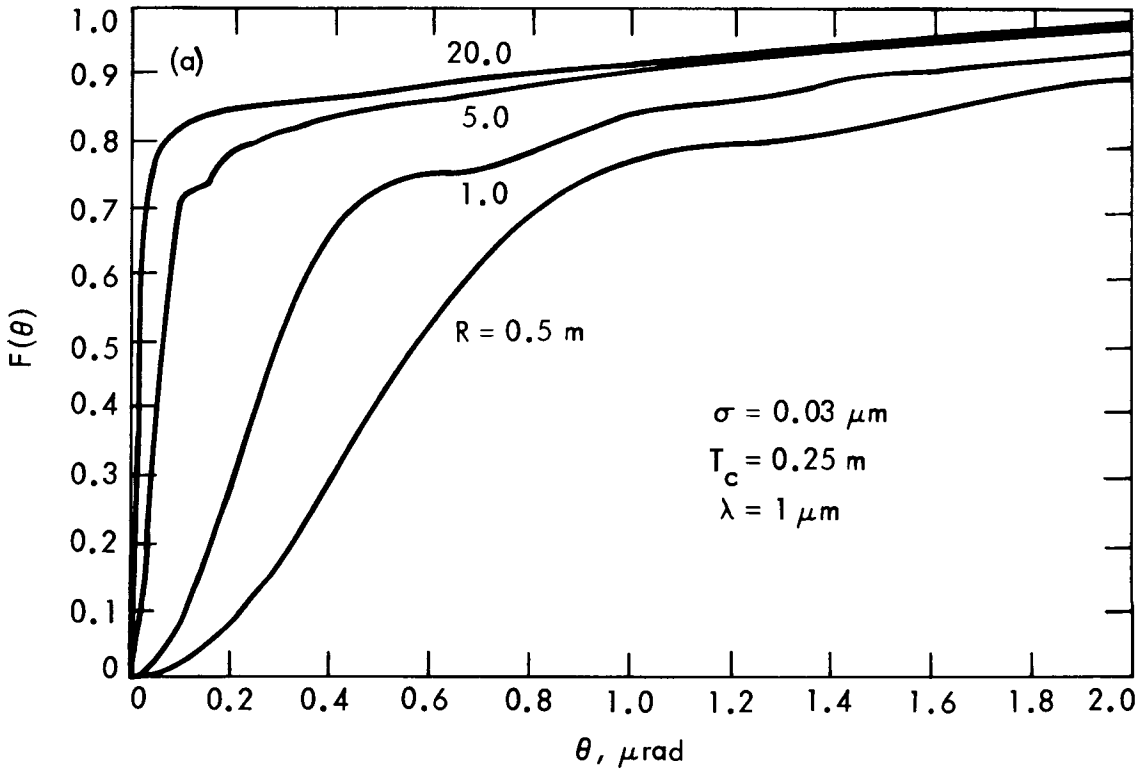

Figure 2-2. Fractional Signal Power F(θ) as a Function of θ for Various System Parameters: (a) σ = 0.03 μm, T_c = 0.25 m, and λ = 1 μm

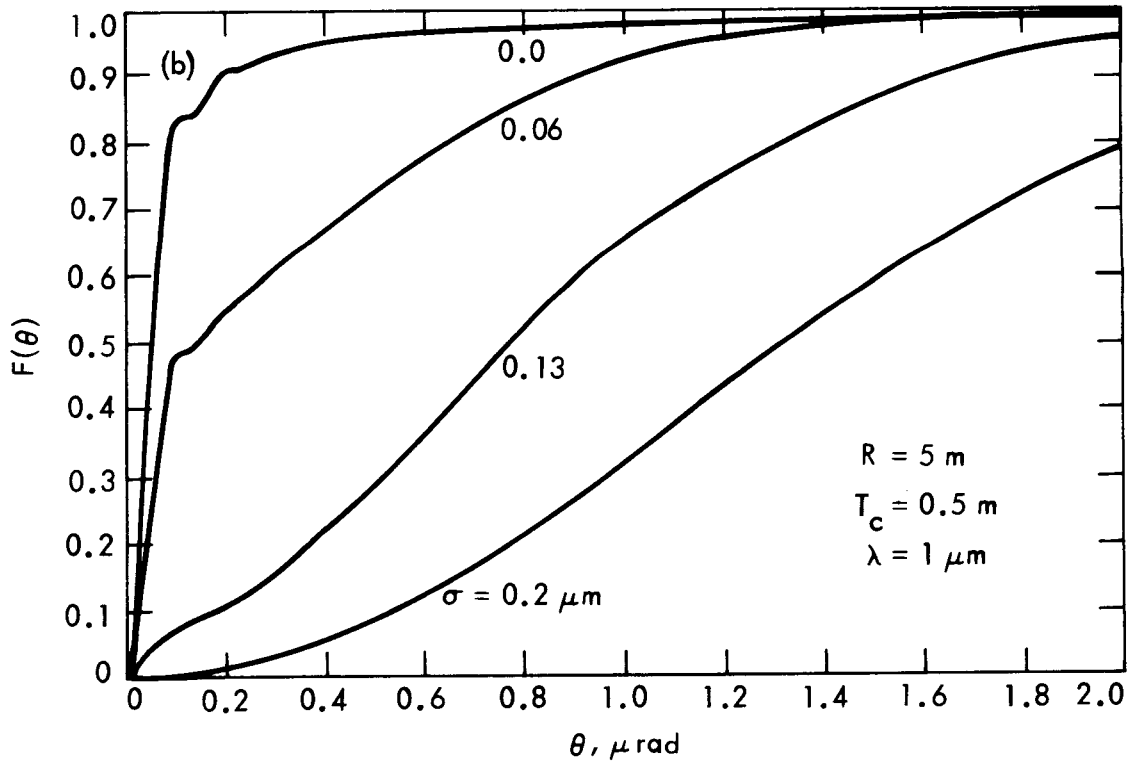

Figure 2-2. Fractional Signal Power F(θ) as a Function of θ for Various System Parameters: (b) R = 5 m, T_C = 0.5 m, and λ = 1 μm

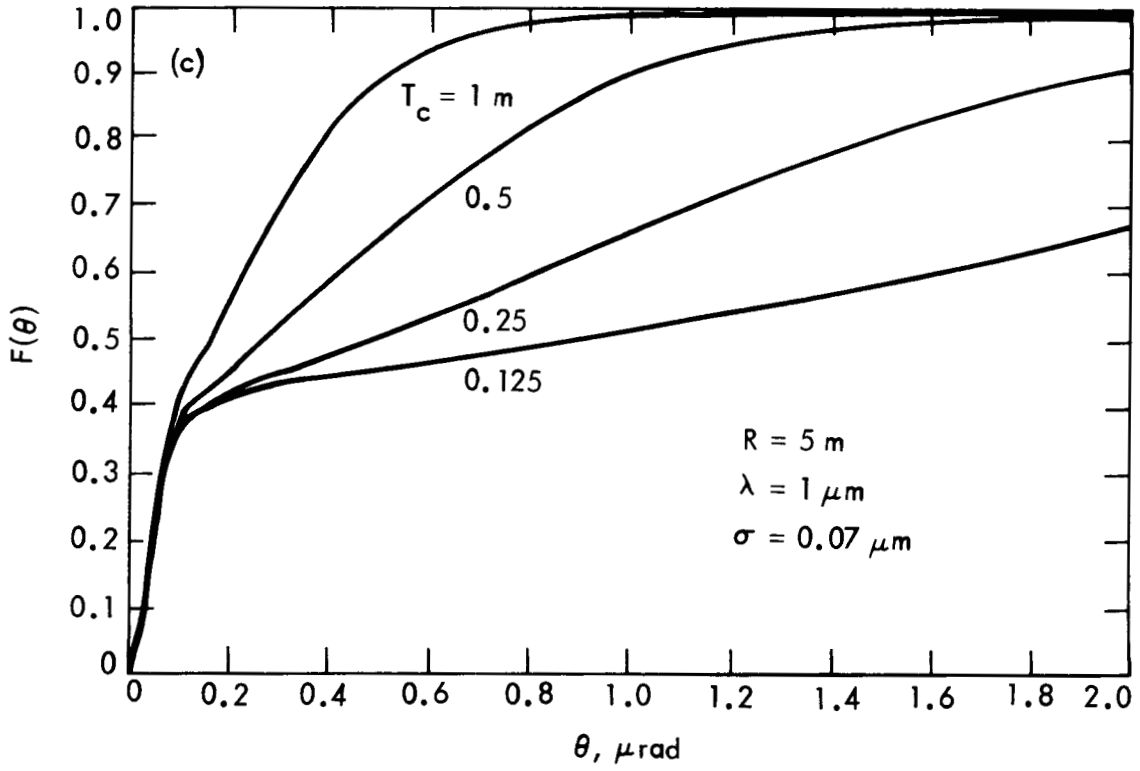

Figure 2-2. Fractional Signal Power F(θ) as a Function of θ for Various System Parameters: (c) σ = 0.07 μm, R = 5 m, and λ = 1 μm

distribution in the focal plane due to a spatially constant background source is also constant; hence the background power passing through a circular aperture of radius θf in the focal plane (over the wavelength range $[\lambda, \lambda + \Delta\lambda)$) becomes

$$P_b(\theta) = \left(A_r \int_{\lambda}^{\lambda+\Delta\lambda} N(\zeta)\, d\zeta \right) \pi\, \theta^2;\ \theta << 1 \text{ rad} \tag{2.6}$$

in watts. Note that the background power reaching the detector array continues to increase with θ, whereas the power due to a normally incident plane-wave reaches its maximum value as $F(\theta)$ approaches one.

An optical detector suitable for photon-counting applications generates an electrical signal that can be related to the number of photons detected in a given time interval. If an optical plane-wave of intensity I_r W/m^2 is normally incident on the reflector, then the average number of photons detected by a centered, circular detector element of radius θf over the time interval $[t, t + \Delta t)$ can be expressed as

$$K_s(\theta) = I_s F(\theta) \tag{2.7}$$

with

$$I_s = \frac{\eta}{h\nu} A_r I_r \Delta t$$

where I_s is the average number of signal photons passing through the receiver's effective aperture in Δt seconds, η is the detector quantum efficiency, and $h\nu$ is the energy of a single photon. Similarly, the average count generated by multimode background radiation over the same time interval in the wavelength range $[\lambda, \lambda + \Delta\lambda)$ becomes

$$K_b(\theta) = I_b \pi \theta^2 \tag{2.8}$$

with

$$I_b = \frac{\eta}{h\nu} A_r \Delta t \int_{\lambda}^{\lambda+\Delta\lambda} N(\zeta) d\zeta$$

in counts/steradian (sr). As an immediate extension of the above results, note that the average count generated by a centered detector-ring of outer radius $\theta_2 f$ and inner radius $\theta_1 f$ is simply $K(\theta_2) - K(\theta_1)$. This expression holds for multi-mode background fields as well as for normally incident plane-waves. In the following sections, the above models will be applied to determine the performance of optical receivers employing rough reflectors, and to develop techniques for improving receiver performance in the presence of interfering background fields.

SECTION 3

OPTICAL RECEIVER PERFORMANCE

3.1 DECODER STRUCTURE

In order to transmit information over the channel, the transmitter modulates the intensity of the transmitted field, which results in a corresponding modulation in the intensity of the received field. For long-distance communications, the received field can be modeled as an intensity-modulated planewave. The receiver bases its decision on a fundamental array of observables, called counts, generated by each element of the detector array over a suitable set of time intervals, in response to the modulated received field. Each time interval should be chosen small enough to ensure that the intensity of the received field remains essentially constant over that interval. Consider a situation in which the transmitter sends one of M waveforms during every signal interval. Then, if each of M received symbols lasts exactly T seconds, N photodetectors responding to both signal and background fields over L time intervals (whose union comprises the interval [0,T)) generate the count array

$$[k] = \begin{bmatrix} k_{11} & \cdots & k_{1L} \\ \vdots & & \\ k_{N1} & \cdots & k_{NL} \end{bmatrix} \tag{3.1}$$

where, under hypothesis "i" (or H_i), the count $k_{\ell n}$ is a Poisson distributed random variable with average value

$$K_{\ell n}^{i} = K_{\ell n}^{i,s} + K_{\ell n}^{b} \tag{3.2}$$

(Here $K_{\ell n}^{i,s}$ refers to the average count due to the signal under H_i, and $K_{\ell n}^{b}$ is the average count due to the background radiation over the n^{th} detector element and ℓ^{th} time interval. The dependence on θ has been suppressed for the sake of notational simplicity.)

Since Poisson counts generated by a deterministic signal field or multimode background radiation over disjoint space (or time) intervals are independent random variables, it follows that the joint probability density of the elemental counts, conditioned on hypothesis "i" being true, can be expressed as

$$P([k] \mid H_i) = \exp\left(-\sum_{\ell=1}^{L}\sum_{n=1}^{N} K_{\ell n}^{i}\right) \prod_{\ell=1}^{L}\prod_{n=1}^{N} \frac{\left(K_{\ell n}^{i}\right)^{k_{\ell n}}}{k_{\ell n}!} \tag{3.3}$$

The "maximum a-posteriori" (MAP) decoder selects the hypothesis with the greatest probability of occurrence, given the observable array [k]. Using Bayes' rule and keeping only terms that depend on H_i, the decisions can be based on the set of log-likelihood functions $\{D_i\}$, where each element of this set is defined as

$$D_i \triangleq \mathcal{T}_i \left\{\log_e \left(P([k],H_i)\right)\right\} \tag{3.4}$$

Here the truncator $\mathcal{T}_i$ keeps only hypothesis-dependent terms. For each observable array, the MAP decoder computes $\{D_i\}$ and selects H_q if

$$\begin{aligned} D_q &= \max_i \{D_i\} \\ &= \max_i \left\{\log_e P(H_i) - K_s^i + \sum_{\ell=1}^{L}\sum_{n=1}^{N} k_{\ell n} w_{\ell n}^{i}\right\} \end{aligned} \tag{3.5}$$

where i = 1, 2, ..., M.

In case several decision functions are tied for largest, the decoder may employ any predetermined strategy to choose one of the candidate hypotheses. In Equation 3.5, K_s^i and $w_{\ell n}^i$ are defined as

$$K_s^i = \sum_{\ell=1}^{L} \sum_{n=1}^{N} K_{\ell n}^{i,s} \tag{3.6a}$$

and

$$w_{\ell n}^i = \log_e \left(1 + \frac{K_{\ell n}^{i,s}}{K_{\ell n}^b}\right) \tag{3.6b}$$

Therefore, the MAP decision is based on the a priori probabilities $P(H_i)$, the total signal energy K_s^i, and a weighted sum of counts obtained from every detector element over the entire observation interval.

The decision function simplifies for the case of equilikely, equal-energy M-ary pulse-position modulated (PPM) signals. For this modulation format, a τ-second optical pulse in the i^{th} τ-second time slot ($\tau \triangleq T/M$) represents hypothesis "i" [Ref. 3]. Now $L = M$, $P(H_i) = 1/M$, and $K_s^i = K_s$ (since $K_{\ell n}^{i,s} = K_n^s$, independent of "i"). Furthermore, it can be seen from Equations 3.2 and 3.6b that if $K_{\ell n}^b$ does not depend on "ℓ", then

$$w_{\ell n}^i = \begin{cases} w_n & ; \quad i=\ell \\ 0 & ; \quad i\neq\ell \end{cases} \tag{3.7}$$

Hence the decision functions reduce to

$$D_i = \sum_{n=1}^{N} k_{in} w_n \tag{3.8}$$

where $i = 1, 2, \ldots, M$.

In this case, the decision is based on the sum of weighted Poisson counts from all detector elements over each time interval $[(i-1)\tau, i\tau)$, and the hypothesis corresponding to the time interval containing the greatest weighted sum is selected.

Since each decision function is a discrete sum, several decision functions may take on the same maximum value with nonzero probability. When this occurs, the problem can be resolved by making a random choice among the decision functions, or by any other strategy that selects a hypothesis corresponding to one of the largest values. Decoder performance is not affected by the particular strategy employed to resolve ties.

3.2 DECODER PERFORMANCE

Prior to observation, each decision function is a random variable, since the individual counts are random variables. The statistics of the counts depend on which hypothesis is actually true. Given that H_q is true, the probability of a correct decision is the probability that D_q exceeds all other D_i $(i \neq q)$, plus the probability that the correct hypothesis is selected when several decision functions are tied for largest. In order to compute the average probability of a correct decision, the probability density of each decision function must be known. If the conditions of Equation 3.8 are satisfied, then the conditional probability density of the i^{th} decision function, D_i, given that H_q is true, can be expressed as

$$p_{D_i}(\alpha|H_q) = \sum_{k=0}^{\infty} p_k(i,H_q)\ \delta(\alpha - \alpha_k) \tag{3.9}$$

As explained in Appendix A, $p_k(i,H_q)$ is the probability mass over the point α_k, when H_q is true and when the weights are according to H_i.

When N detectors are used to observe M-ary symbols, the average probability of a correct decision is

$$_N P_M(C) = \sum_{q=1}^{M} {}_N P_M(C,H_q) \tag{3.10}$$

If equilikely, equal-energy M-ary PPM symbols are transmitted, then by symmetry

$$\begin{aligned} {}_N P_M(C) &= {}_N P_M(C|H_q) \\ &= \left\{ \sum_{r=0}^{M-1} \left(\frac{1}{r+1}\right) \binom{M-1}{r} \sum_{k=1}^{\infty} p_k(q,H_q) \left[p_{\substack{k \\ i\neq q}}(i,H_q) \right]^r \left[\sum_{\substack{j=0 \\ i\neq q}}^{k-1} p_j(i,H_q) \right]^{M-r-1} \right\} \\ &\quad + M^{-1} \left(p_o(q,H_q) \left[p_{\substack{o \\ i\neq q}}(i,H_q) \right]^{M-1} \right) \end{aligned} \tag{3.11}$$

If a single detector is employed, then for Poisson distributed counts, Equation 3.11 becomes

$$\begin{aligned} {}_1 P_M(C) = \Bigg\{ & \sum_{r=0}^{M-1} \left(\frac{1}{r+1}\right) \binom{M-1}{r} \sum_{k=1}^{\infty} \frac{(K_s+K_b)^k}{k!} e^{-(K_s+K_s)} \left[\frac{K_b^k}{k!} e^{-K_b} \right]^r \times \\ & \left[\sum_{j=0}^{k-1} \frac{K_b^j}{j!} e^{-K_b} \right]^{(M-r-1)} \Bigg\} + M^{-1} e^{-(K_S+MK_b)} \end{aligned} \tag{3.12}$$

(K_s and K_b are the average signal and background generated counts, respectively, in each τ-second time interval.) Note that as K_b approaches zero, the average symbol error probability reduces to

$$ {}_1P_M(E) = 1 - {}_1P_M(C) = \left(\frac{M-1}{M}\right) e^{-K_s}; \quad K_b \to 0 \tag{3.13} $$

which is just the probability of erring when attempting to decide between M empty slots by random choice.

3.3 BOUNDS AND APPROXIMATIONS

It is apparent from Equation 3.2 that the average count generated by any detector element is always at least as great as the average count induced by the background radiation. As the smallest element of $[K^b_{\ell n}]$ increases, the envelope of the density of each elemental count approaches a Gaussian density with mean and variance both equal to the particular count-average [Ref. 4]. Thus, for large background levels, each detector output can be modeled as a Gaussian random variable. Since the sum of independent weighted Gaussian random variables is also Gaussian, the envelope of the probability density of the weighted sum defined in Equation 3.8, approximated as a continuous Gaussian random variable, becomes

$$ p_{D_i}(\alpha | H_q) \simeq (2\pi\sigma_i^2)^{-\frac{1}{2}} e^{-(\alpha - \alpha_i)^2/2\sigma_i^2} \tag{3.14} $$

where, for equilikely, equal-energy M-ary PPM signals

$$ \overline{\alpha}_i = \begin{cases} \sum_{n=1}^{N} K_n^b w_n & ; \quad i \neq q \\ \sum_{n=1}^{N} \left(K_n^b + K_n^s\right) w_n & ; \quad i = q \end{cases} \tag{3.15a} $$

and

$$\sigma_i^2 = \begin{cases} \sum_{n=1}^{N} K_n^b w_n^2 & ; \quad i \neq q \\ \sum_{n=1}^{N} \left(K_n^b + K_n^s\right) w_n^2 & ; \quad i = q \end{cases} \tag{3.15b}$$

In the above equations, K_n^b is the average count due to background radiation, K_n^s the average count due to signal, and w_n the weighting factor associated with the n^{th} detector element. Ignoring count equalities, the average probability of a correct decision becomes

$${}_N P_M(C) = {}_N P_M(C|H_q) \simeq$$

$$\int_{-\infty}^{\infty} d\alpha \, \frac{e^{-(\alpha-\bar{\alpha}_q)^2/2\,\sigma_q^2}}{\sqrt{2\pi\,\sigma_q^2}} \left\{ \int_{-\infty}^{\alpha} \frac{e^{-(\beta-\bar{\alpha}_i)^2/2\,\sigma_i^2}}{\sqrt{2\pi\,\sigma_i^2}} \, d\beta \right\}^{(M-1)} \tag{3.16}$$

$$i \neq q$$

which yields, after some manipulation,

$${}_N P_M(E) \simeq$$

$$1 - \int_{-\infty}^{\infty} dy \, \frac{e^{-y^2/2}}{\sqrt{2\pi}} \left\{ 1 - \frac{1}{2} \, \mathrm{Erfc}\left(\frac{\sigma_q}{\sigma_i} y + \frac{(\bar{\alpha}_q - \bar{\alpha}_i)}{\sigma_i} \right) \right\}^{(M-1)} \tag{3.17}$$

$$i \neq q$$

This last expression is considerably easier to evaluate numerically than the exact expression given by Equation 3.11, and can therefore be used to approximate the average symbol-error probability when the intensity of the background radiation is sufficiently great. The accuracy of this approximation under various operating conditions will be examined in the following section.

The performance of the single-detector receiver observing equilikely, equal-energy M-ary PPM signals can be bounded by the inequality

$$ {}_1P_M(E) \leq (M-1)\,{}_1P_2(E) \tag{3.18} $$

which is proven in Appendix B.

The single-detector binary error probability can be expressed as [Ref. 5]

$$ {}_1P_2(E) = e^{-\Delta^2}\left\{\sum_{n=0}^{\infty}\left(\frac{\sqrt{K_b}}{\Delta+\sqrt{K_b}}\right)^n F_n(\psi) - \frac{1}{2}F_o(\psi)\right\} \tag{3.19} $$

where $\Delta = \sqrt{K_s + K_b} - \sqrt{K_b}$, $\psi = 2\sqrt{(K_s + K_b)K_b}$, and $F_n(\psi) = e^{-\psi}I_n(\psi)$. Since for any $\psi \geq 0$ and $n \geq 0$, $I_n(\psi) \leq I_o(\psi)$, it follows that

$$ \begin{aligned} {}_1P_2(E) &\leq e^{-\Delta^2}\left\{\sum_{n=0}^{\infty}\left(\frac{\sqrt{K_b}}{\Delta+\sqrt{K_b}}\right)^n - \frac{1}{2}\right\} F_o(\psi) \\ &= e^{-\Delta^2}\left[\frac{\sqrt{K_b}}{\Delta} + \frac{1}{2}\right] F_o(\psi) \\ &\triangleq {}_1P_2^u \end{aligned} \tag{3.20} $$

The upper bound on the binary PPM error probability, ${}_1P_2^u$, can itself be approximated accurately in the limit of small or large K_b. Thus, for $K_b \ll 1$,

$$ {}_1P_2^u \simeq \frac{1}{2}e^{-\Delta^2} \quad ; \quad K_b \ll 1 \tag{3.21a} $$

while for $K_b \gg 1$, we have

$$ {}_1P_2^u \simeq \left(\frac{\sqrt{K_b}}{\Delta} + \frac{1}{2}\right)\frac{e^{-\Delta^2}}{\sqrt{2\pi\,\psi}} \quad ; \quad K_b \gg 1 \tag{3.21b} $$

The approximation in Equation 3.21b generally yields accurate results even for moderate values of K_b (that is, $K_b \gtrsim 1$). These approximations can be easily evaluated with a calculator to provide the designer with quick, accurate estimates of receiver performance.

SECTION 4

NUMERICAL RESULTS

4.1 RECEIVER PERFORMANCE

In Section 3 we showed that the error probability expressions (as well as the bounds and approximations) depend on the average signal and background counts generated by the detector elements over the signal interval. For a given wavelength (henceforth we assume that λ = 1 μm), the average signal and background counts, K_s and K_b, in turn depend on the reflector parameters σ, T_c, and R, and on the angle θ (which defines the receiver's field-of-view), as was shown in Section 2. In general, θ has to be optimized to achieve best performance (that is, lowest error probability) as the various system parameters are changed. Next we examine the performance of an optical receiver observing M-ary PPM signals, for various reflector parameters and background environments.

4.1.1 No Background Radiation

First consider the limiting case $K_b = 0$, and define K_{so} as the average signal count over the entire detector-plane. In this case no advantage can be gained by using multiple detectors; hence, we need only consider the single detector case (N = 1). Now ${}_NP_M(E)$ is a function of R, σ, T_c, M, K_{so}, and θ. The variation of ${}_NP_M(E)$ with θ for several values of σ is shown in Figure 4-1, with R = 20 m, T_c = 1 m, M = 32, and K_{so} = 10. The limiting error probability of $((M - 1)/M)\exp(-K_{so})$ can be approached arbitrarily closely by increasing θ for any choice of σ; however, it is approached most rapidly by the diffraction-limited reflector (σ = 0.0μm). Therefore, in the absence of background radiation, the only disadvantage of poor reflector surface quality

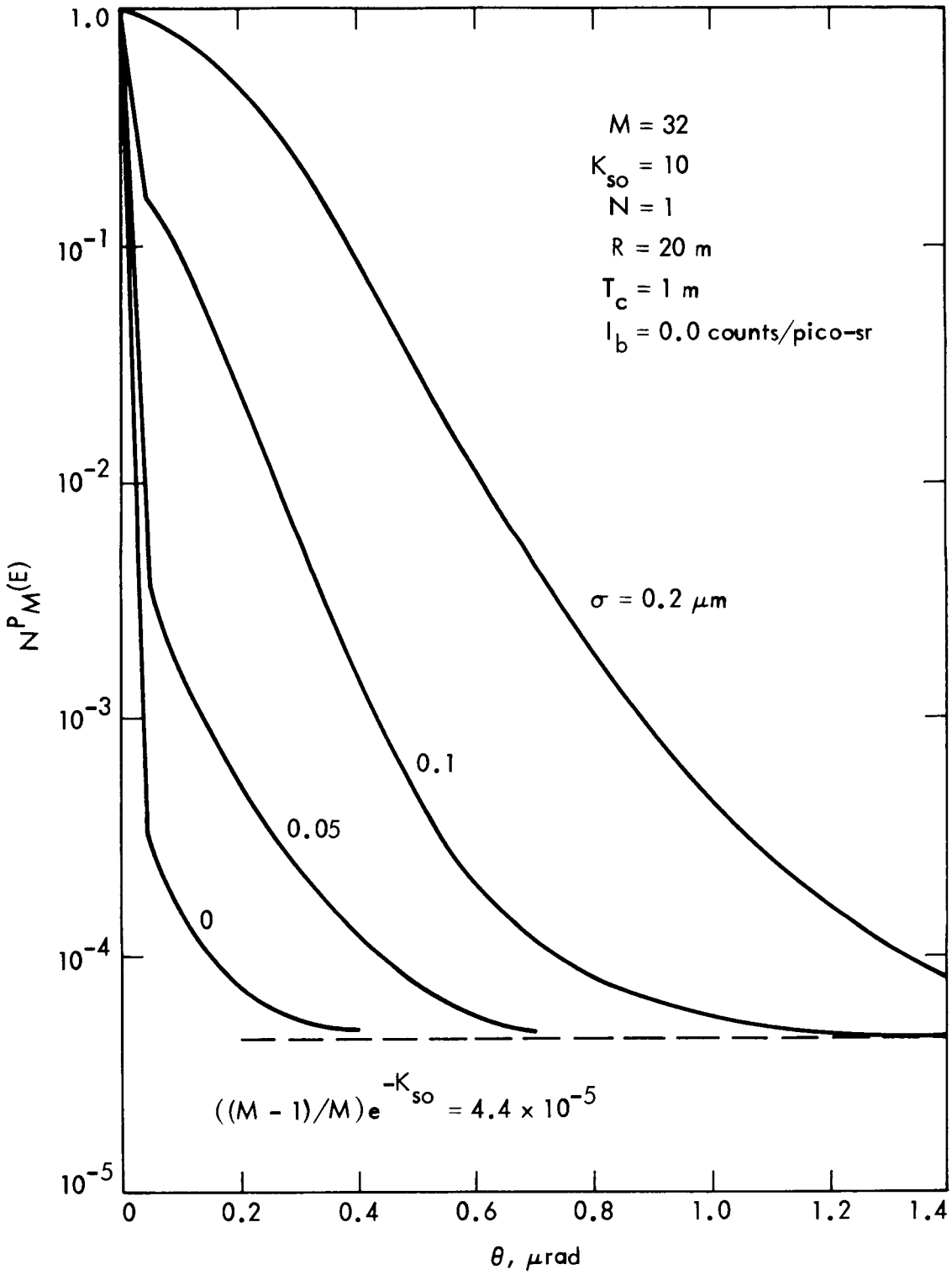

Figure 4-1. Symbol Error Probability $_NP_M(E)$ as a Function of θ, with No Background Radiation

is that the larger field-of-view required to achieve a given performance level increases the chance that nearby stars, or other background sources, might enter the receiver's field-of-view.

4.1.2 The Effects of Background Radiation

As the background level I_b increases from zero, optimization over θ becomes necessary to minimize the error probability. (The units of I_b are counts per 10^{-12} steradians, or counts/pico-sr, referenced to an arbitrary timeslot. Hence, the average noise-count observed over any M-ary time-slot is taken to be $K_b = I_b \pi \theta^2$.) This relationship between θ and I_b is illustrated in Figure 4-2, where the optimum θ, θ_o, is displayed for various background levels, with the other relevant parameters held fixed (K_{so} = 10, R = 20 m, T_c = 1 m, σ = 0.1 μm, and M = 32). The dependence of θ_o on I_b is quite evident from this figure: when the background level is increased, the optimum angle, θ_o, decreases as the receiver attempts to exclude the interfering background radiation while collecting signal energy. However, the minimum error probability also increases with background level, because even with an optimized field-of-view, less signal energy is collected in a noisier environment.

The minimum symbol error probability is shown in Figure 4-3 as a function of K_{so} for various background levels and rms surface deviations (R = 20 m and T_c = 1 m). A single circular detector of radius $\theta_o f$ is used in both cases (of course, θ_o is a function of both I_b and σ, and hence must be determined separately for each computed point on these graphs). Note the rapid performance degradation as the rms surface deviation increases, even for the relatively low background level represented by I_b = 0.04 counts/pico-sr (this level corresponds roughly to an average of 0.13 counts for a field-of-view half-angle of θ = 1 μrad).

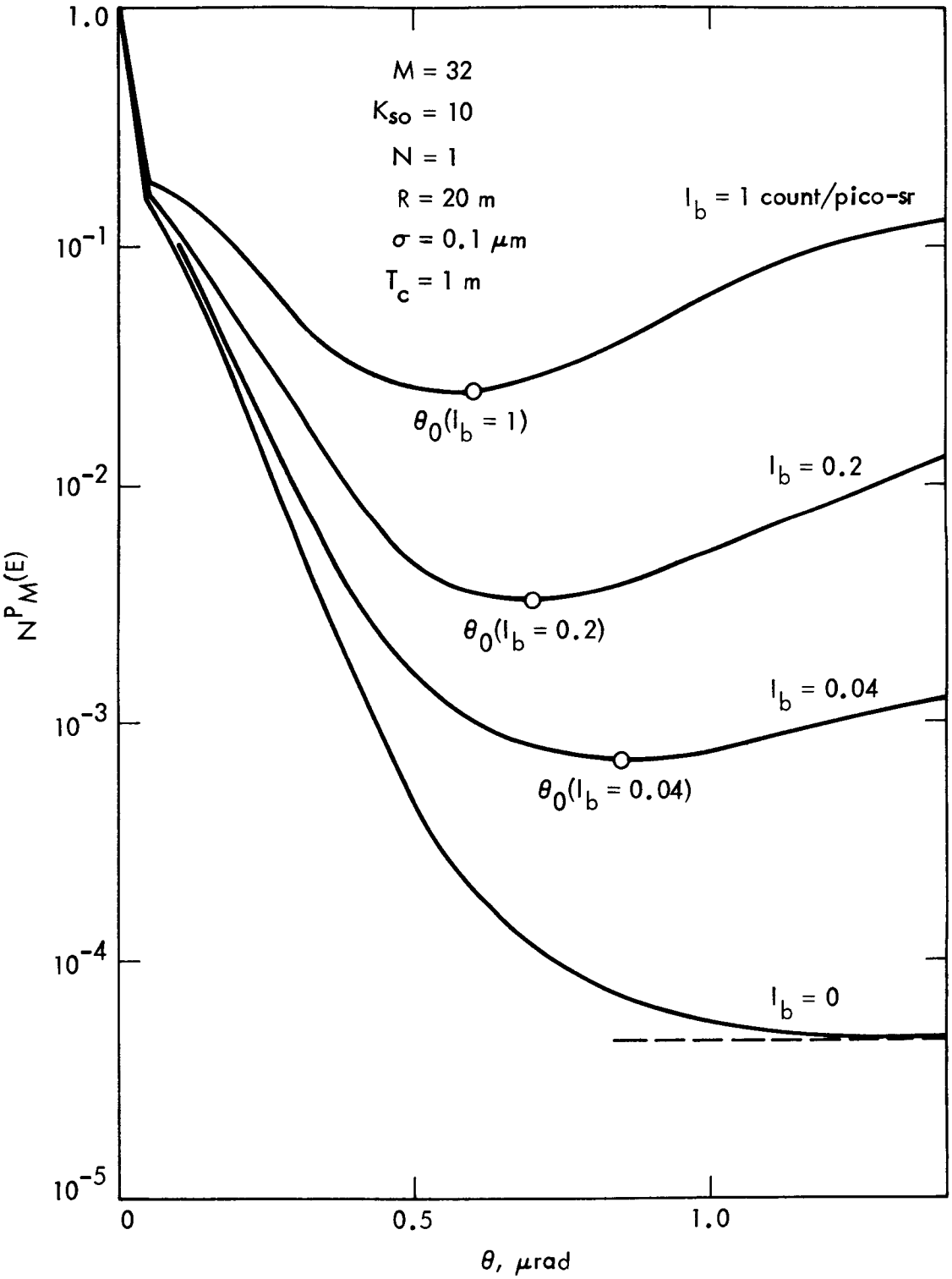

Figure 4-2. Symbol Error Probability ${}_{N}P_{M}(E)$ as a Function of θ in the Presence of Background Radiation

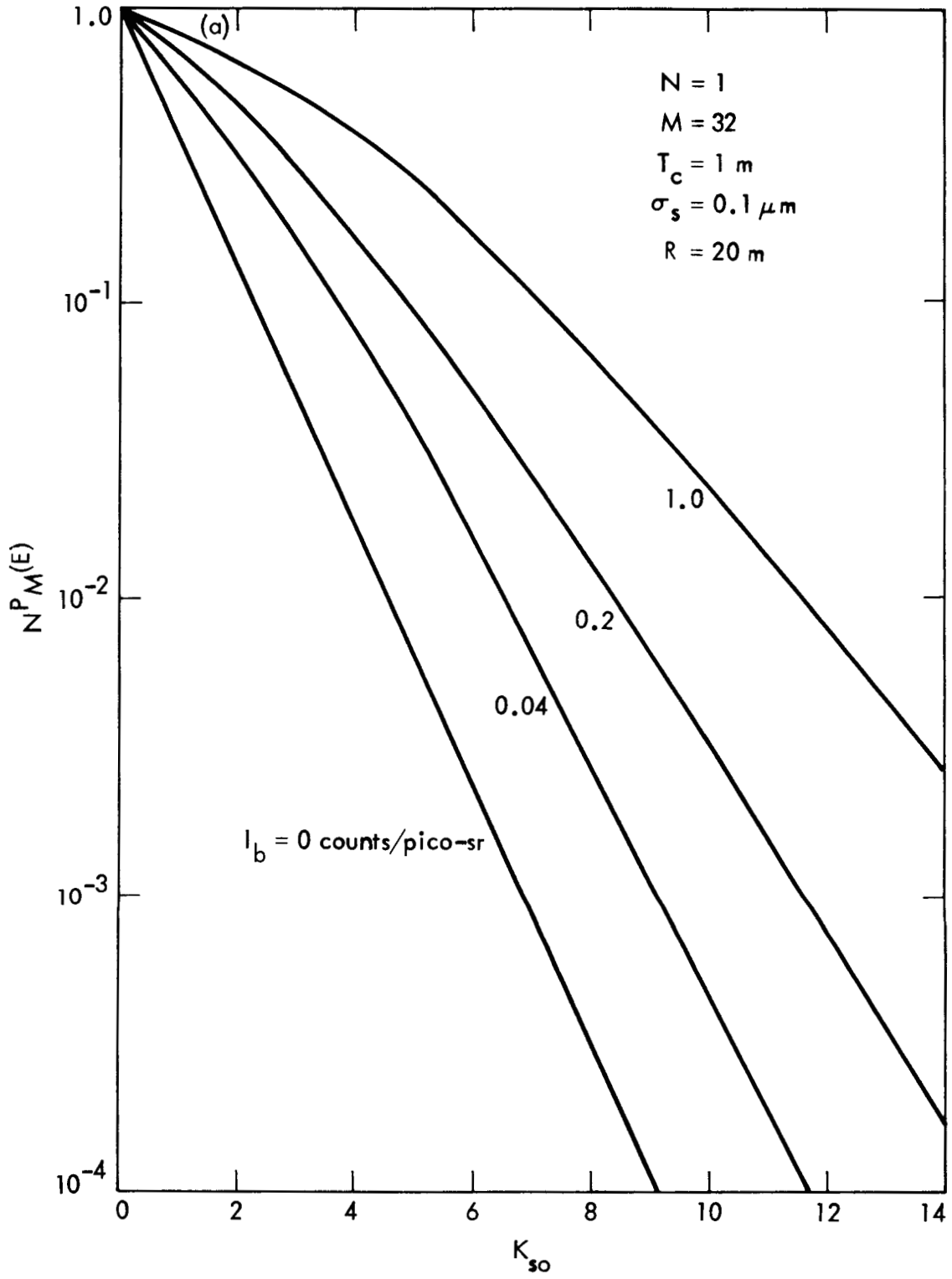

Figure 4-3. Minimum Symbol Error Probability as a Function of K_{so} for: (a) Various Background Levels

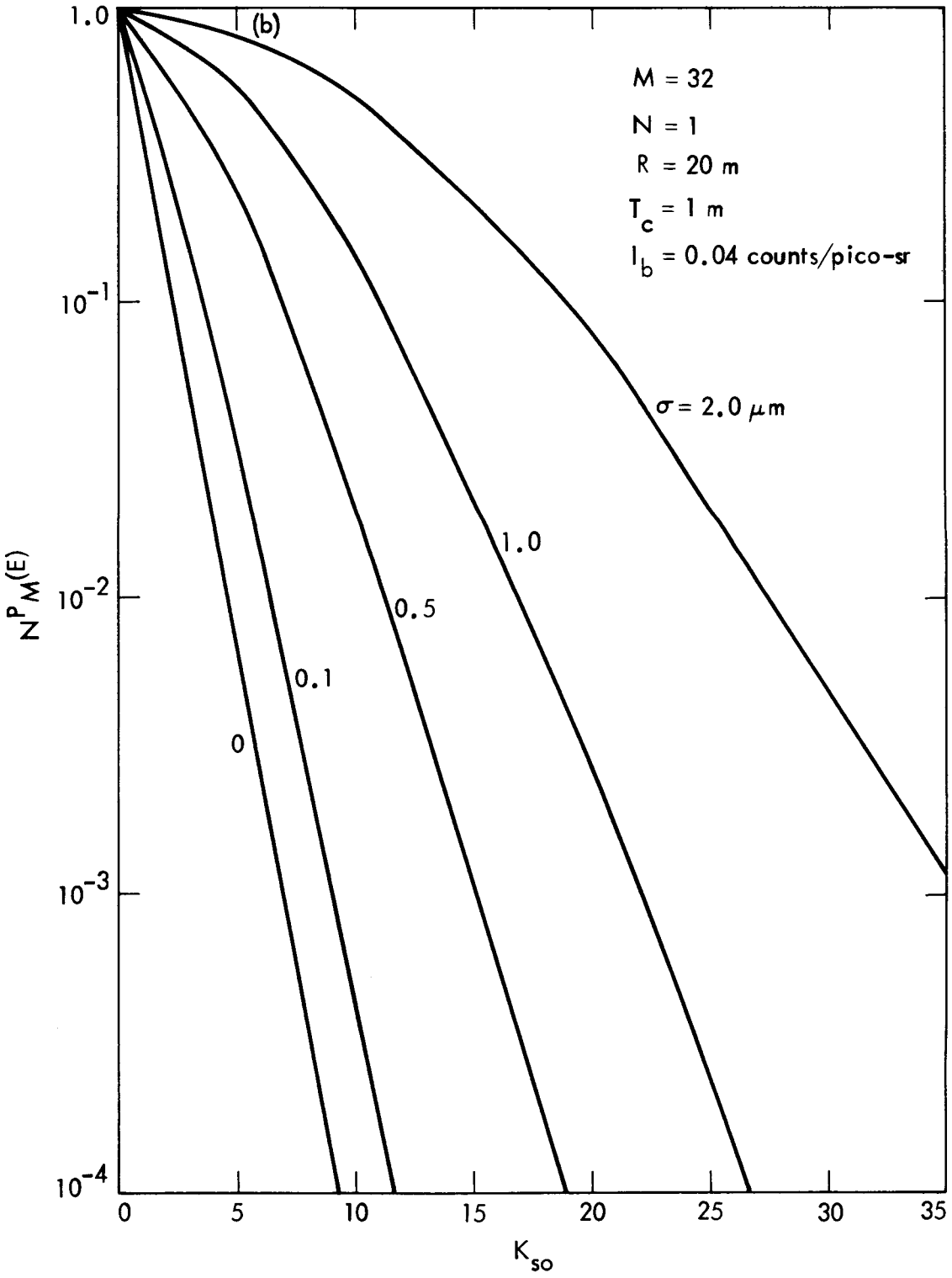

Figure 4-3. Minimum Symbol Error Probability as a Function of K_{so} for: (b) Various rms Surface Deviations

4.1.3 Focal-Plane Detector Arrays

In high background radiation environments, receiver performance can often be improved by using several detector elements to partition the field-of-view, followed by the MAP processing developed in Section 3. For the circularly symmetric signal intensity distributions under consideration, the detector elements take the form of concentric rings designed to collect signal energy from roughly equal-intensity contours in the focal plane. The output of each detector element is multiplied by the appropriate weighting factor (Equation 3.6b) and summed to obtain the decision functions defined by Equation 3.5. Now, Equation 3.11 must be evaluated to determine receiver performance (recall that Equation 3.11 applies only to equilikely, equal-energy M-ary PPM signals). We have seen in Section 2 that the signal intensity distributions under consideration here can be roughly divided into diffracted and scattered components. Therefore, it seems reasonable to divide the field-of-view into two regions by using concentric detector elements matched to each component. The inner detector element (of radius $\theta_1 f$) collects mainly diffracted signal energy, while the outer detector ring (of outer radius $\theta_2 f$ and inner radius $\theta_1 f$) collects scattered signal energy. Best performance is obtained by finding the two radii that minimize the probability of error, subject to the constraint $\theta_2 > \theta_1$. (Of course, further improvements are possible by using more than two detector elements; however, for the type of intensity distributions under consideration, the additional improvement is generally not significant.) The improvement over the optimized single-detector configuration can be seen in Figures 4-4(a) and (b). (Note that in Figure 4-4(a), M = 2.) The greatest relative improvement is obtained in Figure 4-4(a), where most of the signal energy is in the scattered fields, but

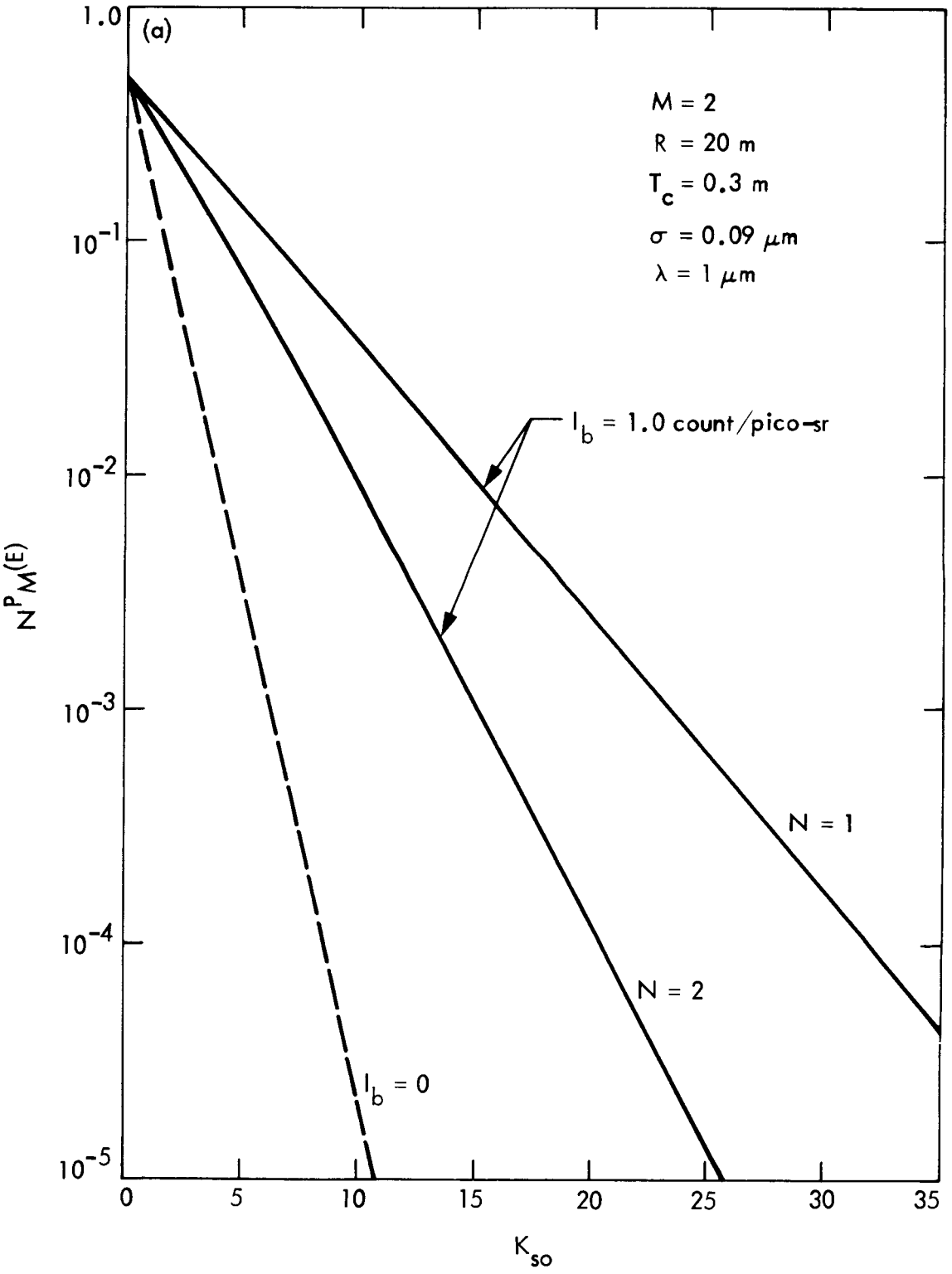

Figure 4-4. Minimum Error Probability as a Function of K_{so} for Optimized Single-Detector (N = 1) and Partitioned Field-of-View (N = 2) with: (a) Moderate Background Level, M = 2

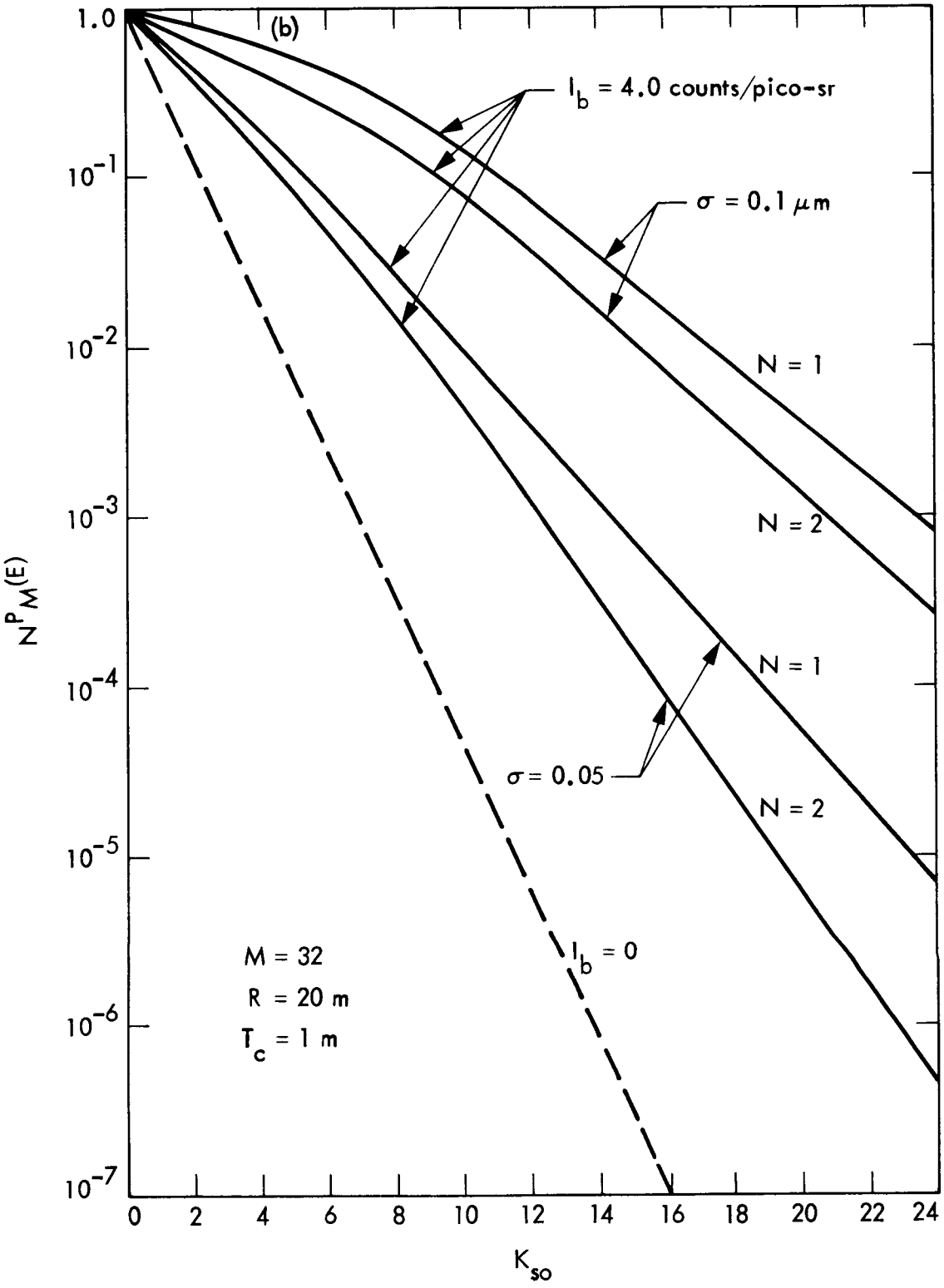

Figure 4-4. Minimum Error Probability as a Function of K_{so} for Optimized Single-Detector (N = 1) and Partitioned Field-of-View (N = 2) with: (b) High Background Level, M = 32

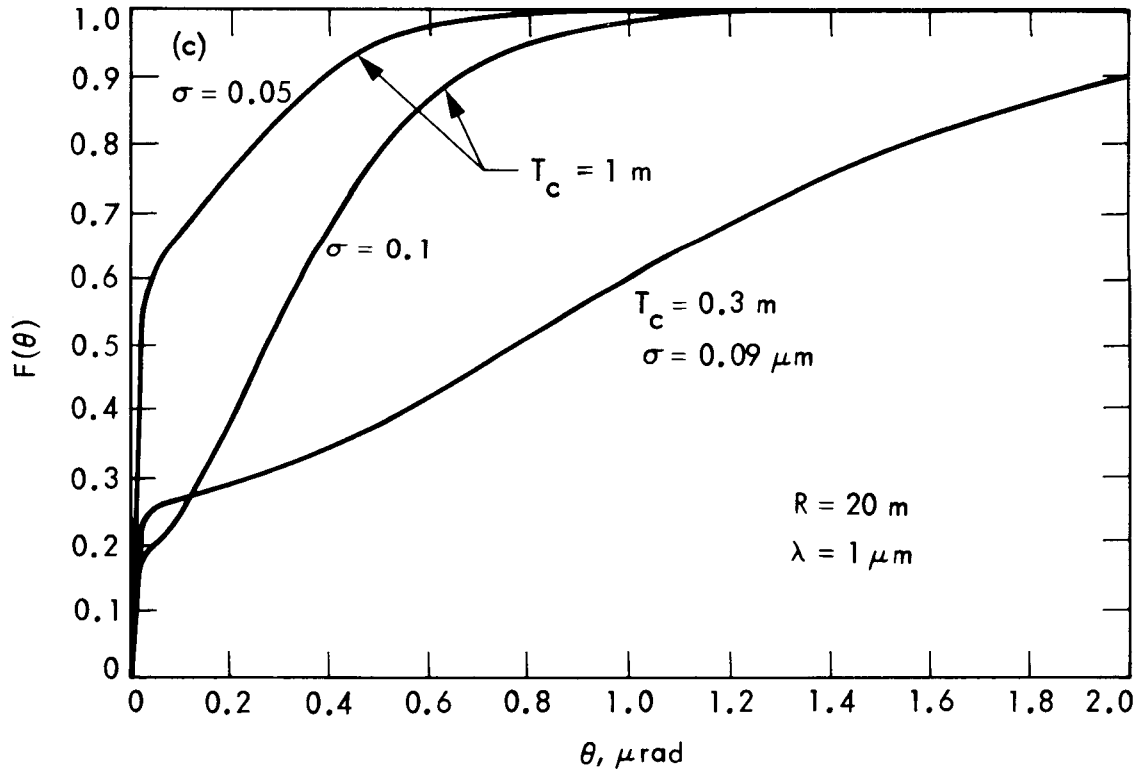

Figure 4-4. Minimum Error Probability as a Function of K_{SO} for Optimized Single-Detector (N = 1) and Partitioned Field-of-View (N = 2) with: (c) Fractional Signal Power vs. θ for Cases Considered in Figures 4-4(a) and (b)

a significant amount of essentially noise-free signal energy remains in the diffracted field. A lower bound on the achievable performance is also shown for comparison ($I_b = 0$). Note that significant signal power savings can be realized by using two detector elements (N = 2) relative to the single-detector case (N = 1), but the noiseless performance bound cannot be reached, even as the number of detectors grows without bound. Less favorable situations are illustrated in Figure 4-4(b), where the noise level, and the distribution of diffracted and scattered signal components are such that no significant advantage can be attained over the optimized single-detector case. The signal intensity distributions corresponding to the performance curves of Figures 4-4(a) and (b) are shown in Figure 4-4(c).

4.2 PERFORMANCE BOUNDS AND APPROXIMATIONS

The bounds and approximations developed in Section 3 can often be used to obtain quick answers without extensive numerical computation. The approximate expression given in Equation 3.17 yields excellent results for both single- and multiple-detector receivers as the background intensity becomes sufficiently great. This approximation is based on the fact that the envelope of the Poisson probability density approaches a Gaussian density as the average count-rate grows without bound. It is apparent from Figure 4-5 that for the single detector case (N = 1), the agreement between the exact solution and the Gaussian approximation is very good when $K_b \gtrsim 10$, but the approximation tends to become unreliable for small background counts (i.e., when $K_b \lesssim 1$). When two (or more) detectors are employed, the Gaussian approximation continues to yield good results as long as all detector elements observe high background counts. In Figure 4-6, condition "A" is defined as $K_{b1} = 10$, $K_{b2} = 5$, $K_{s2} = 2\ K_{s1}$, and condition "B" as $K_{b1} = 2$, $K_{b2} = 1$, $K_{s2} = 2\ K_{s1}$. Note

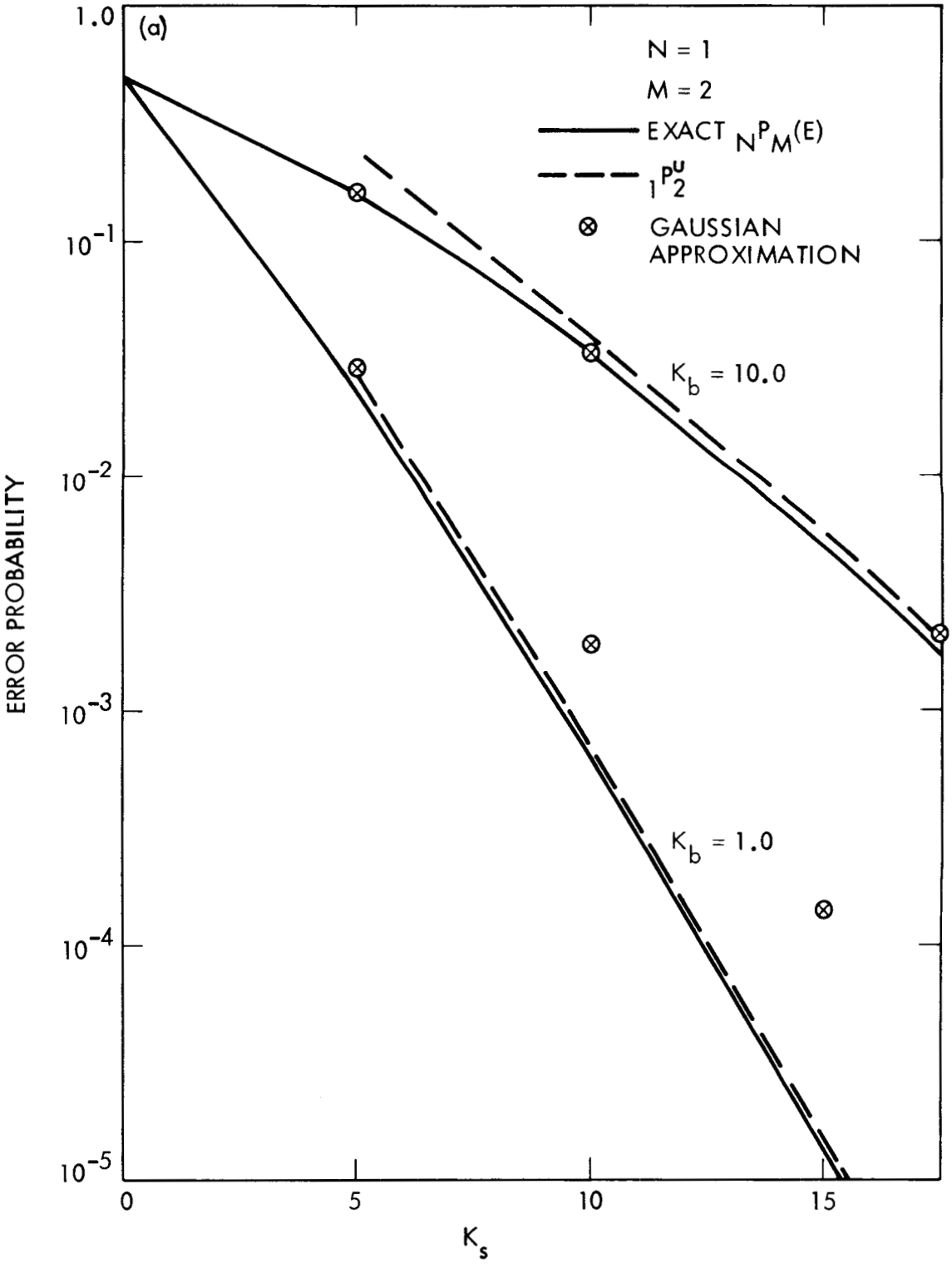

Figure 4-5. Performance Bounds and Approximations with: (a) M = 2

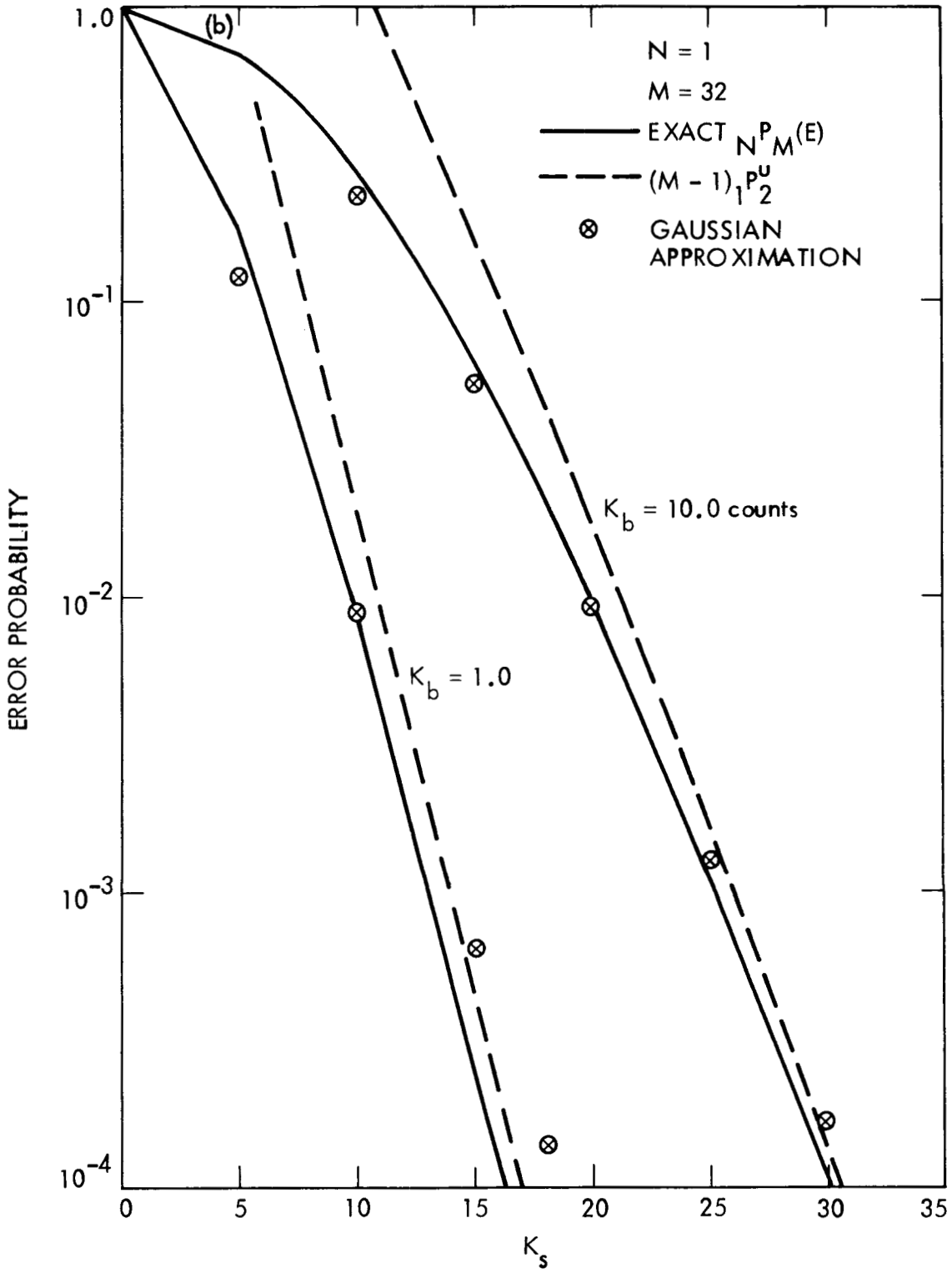

Figure 4-5. Performance Bounds and Approximations with: (b) M = 32

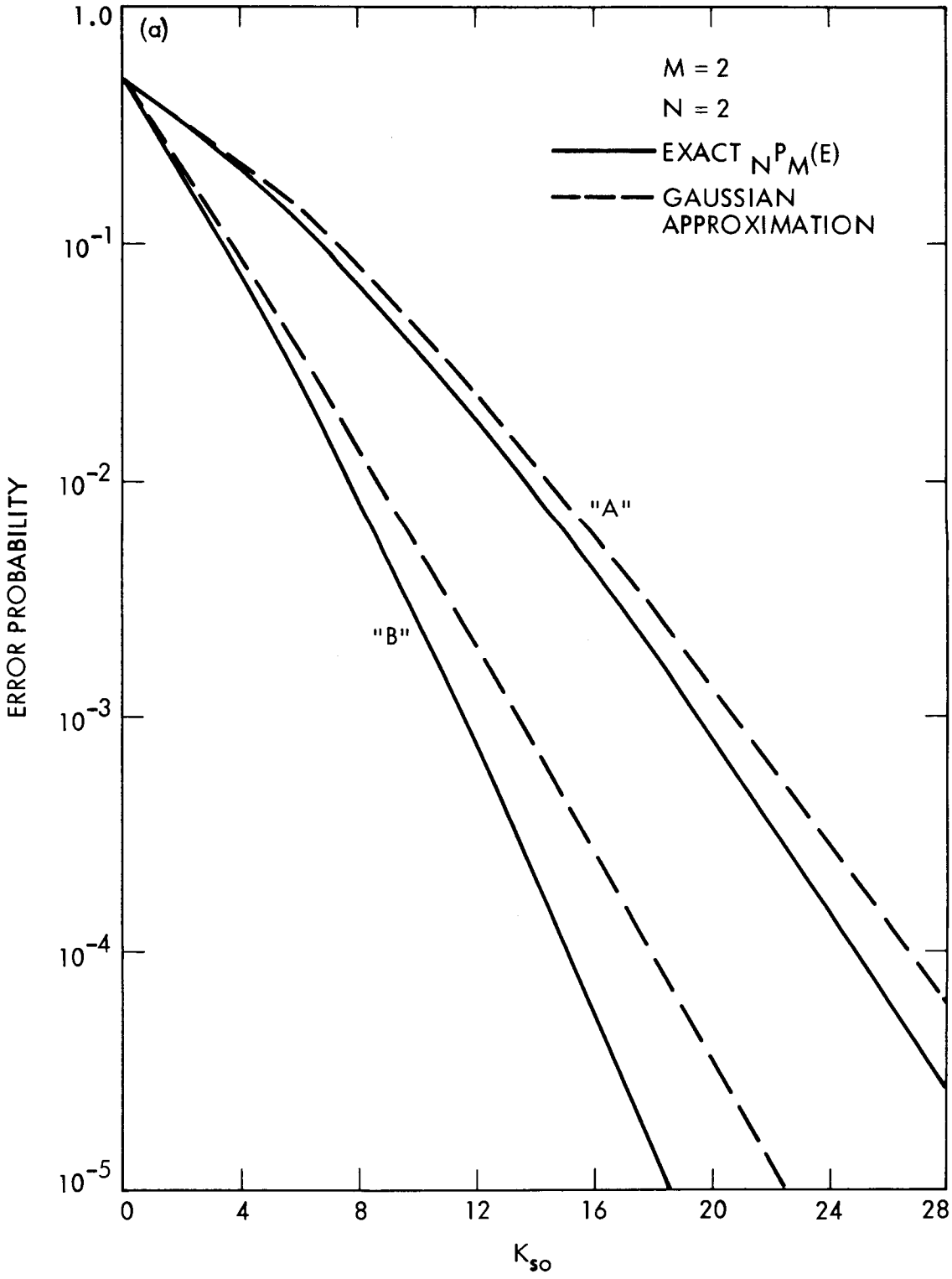

Figure 4-6. Symbol Error Probability Approximations for a Partitioned Field-of-View with: (a) M = 2

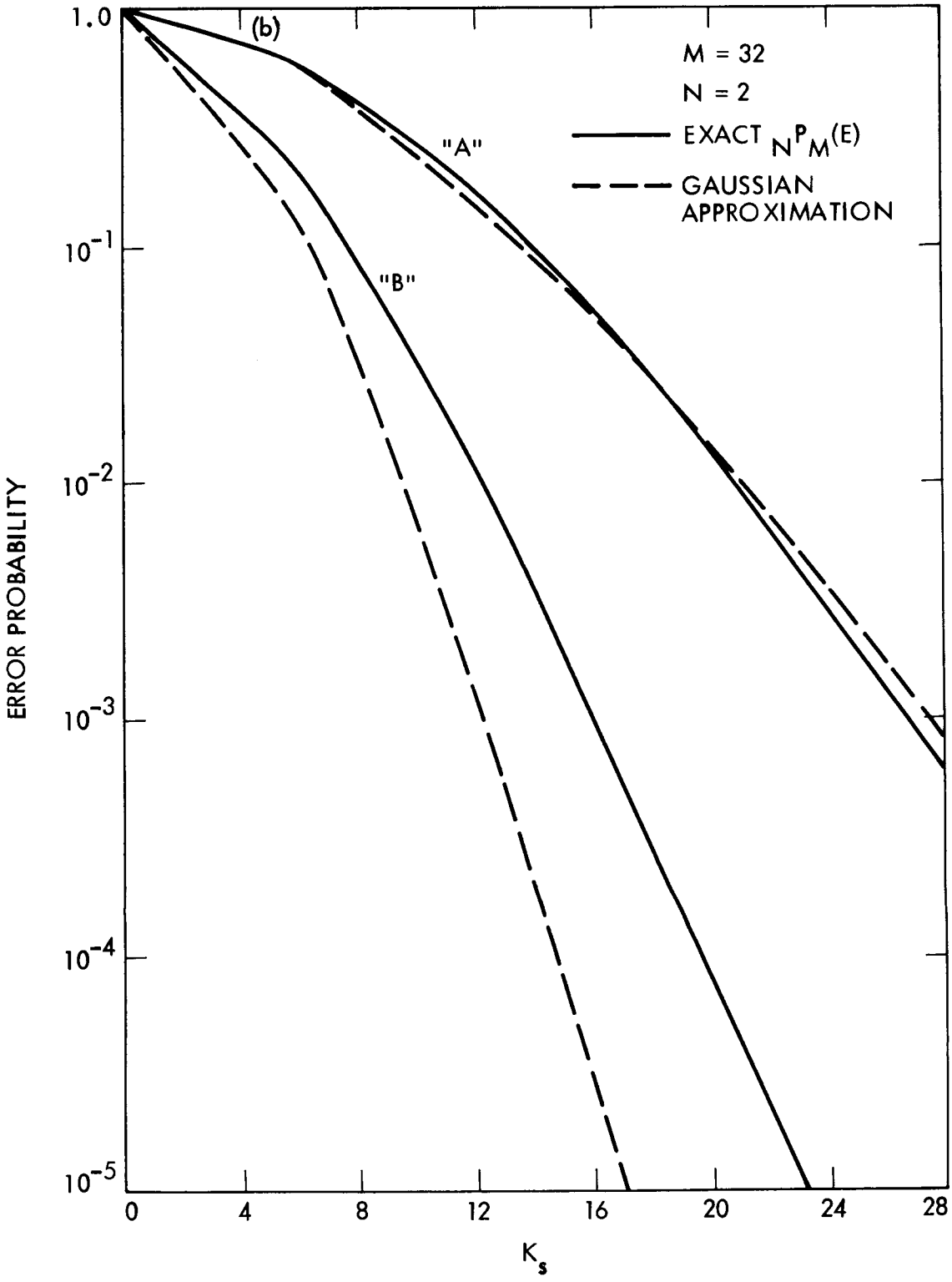

Figure 4-6. Symbol Error Probability Approximations for a Partitioned Field-of-View with: (b) M = 32

that the exact result and the Gaussian approximation are in good agreement under condition "A" for M = 32 as well as for M = 2, but that the approximation tends to become erratic under the weaker background condition, "B." Thus, care must be exercised when using this approximation in regions where the Gaussian assumption may not apply.

The behavior of the binary upper bound ${}_1P_2^u$, defined in Equation 3.20, is shown in Figure 4-5(a) as a function of K_s, for the case of intermediate ($K_b = 1$) and large ($K_b = 10$) background counts. The M-ary bound $(M - 1){}_1P_2^u$ is shown in Figure 4-5(b) for M = 32. It is apparent that these bounds are tight at low error probabilities, for intermediate as well as large background counts. The approximation to the binary bound defined in Equation 3.21b uses the first term of the asymptotic expansion of $I_o(\psi)$; therefore, it is accurate as long as $\psi \gg 1$, a condition that is guaranteed to hold if $K_b \gg 1$. (For the high-background case shown in Figure 4-5, the approximation cannot be distinguished from the bound in the region $K_s \gtrsim 5$.) However, the low background count approximation to the binary bound (Equation 3.21a) should only be used in situations involving extremely low background counts, as it tends to become inaccurate in intermediate-background cases.

SECTION 5

CONCLUDING REMARKS

The possibility of using "rough" reflectors for the purpose of receiving optical signals has been examined in the previous sections. It was shown that reflector surface quality has little effect on receiver performance in the absence of background radiation, as long as the receiver's field-of-view can be increased sufficiently to collect most of the scattered signal energy. However, background radiation may cause serious deterioration in receiver performance when rough reflectors are employed. This problem can be ameliorated by partitioning the receiver's field-of-view to obtain independent samples of the distorted signal field, and resorting to more complicated schemes for processing the field samples to improve receiver performance. It was found that under favorable circumstances adequate performance can often be maintained using nondiffraction-limited receivers, possibly leading to significant savings in cost and receiver complexity. Bounds and approximations to the exact error-probability expressions have also been developed to aid in system design without the need for extensive numerical computation.

SECTION 6

REFERENCES

1. P. Beckmann and A. Spizzichino, "The Scattering of Electromagnetic Waves from Rough Surfaces," Pergammon Press, New York, 1963.
2. T. S. Mast, J. E. Nelson, and W. J. Welch, "The Effects of Primary Mirror Segmentation on Telescope Image Quality," University of California, Berkeley, Ten-Meter Telescope Report No. 68, Lawrence Berkeley Laboratory, Berkeley, California, March 1982.
3. R. M. Gagliardi and S. Karp, Optical Communications, J. Wiley and Sons, New York, 1976.
4. W. B. Davenport, Probability and Random Processes, McGraw Hill, New York, 1970.
5. W. M. Hubbard, "Binary Detection in an Optical Twin Channel Receiver," IEEE Trans. on Comm. Tech., Vol. 19, pp. 221-223, April 1971.

APPENDIX A

In this appendix, a useful form of the conditional probability density of the i^{th} weighted count, given H_q, is derived. Let z_i denote the sum of all elemental counts weighted according to hypothesis "i":

$$z_i = \sum_{\ell=1}^{L} \sum_{n=1}^{N} k_{\ell n} \, w_{\ell n}^{i} \tag{A.1}$$

Since the elemental counts are independent, the characteristic function of z_i can be expressed as the product of the characteristic functions of the individual weighted counts. If the counts are governed by hypothesis "q," then the characteristic function of z_i, given H_q, becomes

$$\phi_{z_i}(\omega|H_q) = \exp\left\{\sum_{\ell=1}^{L} \sum_{n=1}^{N} K_{\ell n}^{q} \left[\exp\left(j\omega \, w_{\ell n}^{i}\right) - 1\right]\right\} \tag{A.2}$$

The conditional probability density of z_i, given H_q, can be expressed as the inverse transform of $\phi_{z_i}(\omega|H_q)$:

$$p_{z_i}(\alpha|H_q) = \frac{1}{2\pi} \int_{-\infty}^{\infty} \phi_{z_i}(\omega|H_q) e^{j\omega\alpha} d\omega \tag{A.3}$$

Note that $p_{z_i}(\alpha|H_q)$ is a discrete density, since it can be viewed as the convolution of a finite number of discrete densities. Therefore, this conditional density can always be expressed as

$$p_{z_i}(\alpha|H_q) = \sum_{k=0}^{\infty} p_k(i, H_q)\ \delta\ (\alpha - \alpha_k^i) \qquad (A.4)$$

where $p_k(i,H_q)$ represents a nonzero probability mass defined over the point $\alpha = \alpha_k^i$. With no loss in generality, we can assume the ordering

$$0 = \alpha_0^i < \alpha_1^i < \alpha_2^i \ \ldots$$

so that for any "i," $\{\alpha_k^i\}$ is an ordered set of points along the nonnegative real line. The value of the probability mass over some point α_k^i depends on the distribution of signal and background energy over the detector array. Given H_q, the values of $p_k(i,H_q)$ can be computed for any k, once the distribution of signal and background energy is specified.

APPENDIX B

This appendix is devoted to the proof of the inequality shown in Equation 3.18. By symmetry, it suffices to prove that

$$ {}_1P_M(E \mid H_1) \leq (M-1)\,{}_1P_2(E \mid H_1) \tag{B.1} $$

Write the conditional error probability as

$$ {}_1P_M(E \mid H_1) = P_{M1} + P_{M2} \tag{B.2} $$

where

$$ P_{M1} = \Pr \{k_2 > k_1 \text{ or } k_3 > k_1 \ldots \text{ or } k_M > k_1 \mid H_1\} $$

and

$$ P_{M2} = \Pr \{\text{committing an error when attempting to resolve ties among maximal counts including the signal count} \mid H_1.\} $$

If

$$ P_{M1} \leq (M-1)P_{21} \tag{B.3a} $$

and

$$ P_{M2} \leq (M-1)P_{22} \tag{B.3b} $$

then it follows that Equation B.1 is true. But Equation B.3a is true because the probability of the union of events is upper-bounded by the sum of the probabilities of the constituent events (union bound). To show that Equation B.3b is true, let

$$x_k = \frac{K_b^{\,k}}{k!} e^{-K_b}$$

and

$$y_k = \sum_{j=0}^{k-1} \frac{K_b^{\,j}}{j!} e^{-K_b}$$

and write P_{M2} as

$$P_{M2} = \sum_{k=0}^{\infty} C(K_b,K_s;k) \left[\sum_{r=1}^{M-1} \left(\frac{r}{r+1}\right) \binom{M-1}{r} x_k^{r-1} y_k^{M-r-1} \right] \qquad (B.4)$$

where

$$C(K_b,K_s;k) = \frac{(K_b+K_s)^k}{k!} e^{-(K_b+K_s)} x_k$$

Since $\Sigma\ C(K_b,K_s;k) = 2\ P_{22}$, it suffices to prove that

$$\sum_{r=1}^{M-1} \left(\frac{r}{r+1}\right) \binom{M-1}{r} x_k^{r-1} y_k^{M-r-1} \leqslant \frac{(M-1)}{2} \qquad (B.5)$$

But

$$\binom{M-1}{r} = \frac{M-1}{r} \binom{M-2}{r-1}$$

Therefore

$$\sum_{r=1}^{M-1} \left(\frac{M-1}{r+1}\right) \binom{M-2}{r-1} x_k^{r-1} y_k^{M-r-1} \leqslant \left(\frac{M-1}{2}\right) \sum_{r=1}^{M-1} \binom{M-2}{r-1} x_k^{r-1} y_k^{M-r-1} =$$

$$\left(\frac{M-1}{2}\right) (x_k+y_k)^{M-2} \leqslant \frac{M-1}{2}$$

Hence Equation B.1 is true as asserted.